Occupational disorder as the origin of flattening of the acoustic phonon branches in the clathrate Ba8Ga16Ge30

Susmita Roy, Tyler C. Sterling, Dan Parshall, Eric Toberer, Mogens Christensen, Devashibhai T. Adroja, and Dmitry Reznik

Occupational disorder as the origin of flattening of the acoustic phonon branches in the clathrate Ba$_8$Ga$_{16}$Ge$_{30}$

Susmita Roy [○],[1] Tyler C. Sterling [○],[1] Dan Parshall,[1,2] Eric Toberer,[3] Mogens Christensen [○],[4]
Devashibhai T. Adroja [○],[5] and Dmitry Reznik [○][1,6,*]

[1]*Department of Physics, University of Colorado Boulder, 390 UCB, Boulder, Colorado 80309, USA*
[2]*Department of Economics, Universidad del Rosario, Calle 12C 6-25, Bogotá, Distrito Capital 111711, Colombia*
[3]*Department of Physics, Colorado School of Mines, 1500 Illinois Street, Golden, Colorado 80401, USA*
[4]*Department of Chemistry and Interdisciplinary Nanoscience Center (iNANO), Aarhus University,*
Langelandsgade 140, Aarhus 8000, Denmark
[5]*ISIS Facility, STF, Rutherford Appleton Laboratory, Chilton 610101, Oxfordshire OX11 0QX, United Kingdom*
[6]*Center for Experiments on Quantum Materials, University of Colorado Boulder, 390 UCB, Boulder, Colorado 80309, USA*

In the search for high-performance thermoelectrics, materials such as clathrates have drawn attention due to having both glasslike low phonon thermal conductivity and crystal-like high electrical conductivity. Ba$_8$Ga$_{16}$Ge$_{30}$ (BGG) has a loosely bound guest Ba atom trapped inside rigid Ga-Ge cage structures. Avoided crossings between acoustic phonons and the flat guest atom branches have been proposed to be the source of the low lattice thermal conductivity of BGG. Ga-Ge site disorder with Ga and Ge exchanging places in different unit cells has also been reported. We used time-of-flight neutron scattering to measure the complete phonon spectrum in a large single crystal of BGG and compared these results with predictions of density functional theory to elucidate the effect of the disorder on heat-carrying phonons. Experimental results agreed much better with the calculation assuming the disorder than with the calculation assuming the ordered configuration. Although the atomic masses of Ga and Ge are nearly identical, we found that disorder strongly reduces phonon group velocities, which significantly reduces thermal conductivity. Our work points to a path towards optimizing thermoelectrics.

Thermoelectric materials enable environmentally friendly waste-heat-to-electricity conversion [1,2]. The efficiency of a thermoelectric is determined by a dimensionless quantity called the figure of merit: ZT $= \sigma S^2 T / \kappa$, in which σ is the electrical conductivity, S is the Seebeck coefficient, T is the temperature, and κ is the thermal conductivity [3]. The thermal conductivity $\kappa = \kappa_L + \kappa_e$ is the sum of the lattice thermal conductivity κ_L and the electronic thermal conductivity κ_e. It is classically known that the lattice component is the relevant one for thermoelectric performance [4]. According to the kinetic theory of gases, κ_L is proportional to the lattice heat capacity C, the average phonon velocity v, and the average relaxation time τ of phonons. In most cases, low, glasslike κ_L is attributed to reduced v and/or τ.

Glasslike low lattice thermal conductivity and crystal-like high electrical conductivity coexist in so-called phonon-glass electron-crystal (PGEC) materials [5]. One way to realize this concept is by designing materials such that loosely bound "guest" atoms sit inside empty spaces of a rigid atomic lattice with good electronic conductivity [6–9]. In this case, interactions between the low-energy rattling motion of the guest atoms and acoustic phonons reduce v and/or τ depending on specific materials. In particular, the reduction of v is achieved through avoided crossings (anticrossings) between low-lying

optic branches with acoustic branches that result from coupling between the phonons in branches that would cross in the absence of such a coupling. In this case the dispersion curves never cross, instead "avoiding" each other. As a result the branches become more flat, and v decreases.

The X_8Ga$_{16}$Ge$_{30}$ $(X = $ Ba, Eu, Sr$)$ clathrates have low lattice thermal conductivity ($\sim$1 W/mK at room temperature), which makes them promising candidates for efficient thermoelectrics [6,10,11]. Their structure is characterized by tetrakaidecahedral $(\mathrm{Ga}, \mathrm{Ge})_{24}$ and dodecahedral cages $(\mathrm{Ga}, \mathrm{Ge})_{20}$ with loosely bonded Ba, Eu, or Sr guest atoms inside, which makes them a classic type of PGEC material [12,13]. Evidence of strong occupational disorder of the Ga and Ge sites has also emerged recently, i.e., Ga and Ge are distributed nearly randomly on the cage vertices [Fig. 1(a)] [14–18]. Since Ga and Ge have similar atomic masses, the effect of their occupational disorder on phonon dispersions was implicitly assumed to be minimal. Here we combined comprehensive time-of-flight (TOF) inelastic neutron scattering measurements of Ba$_8$Ga$_{16}$Ge$_{30}$ with calculations based on density functional theory (DFT) assuming both the ordered and the disordered structures and found that the disorder splits the degenerate rattler branches into multiple nearly flat branches. The new branches produce many more avoided crossings with the acoustic modes, which significantly lowers their average group velocities and, as a consequence, reduces thermal conductivity. Our result demonstrates that
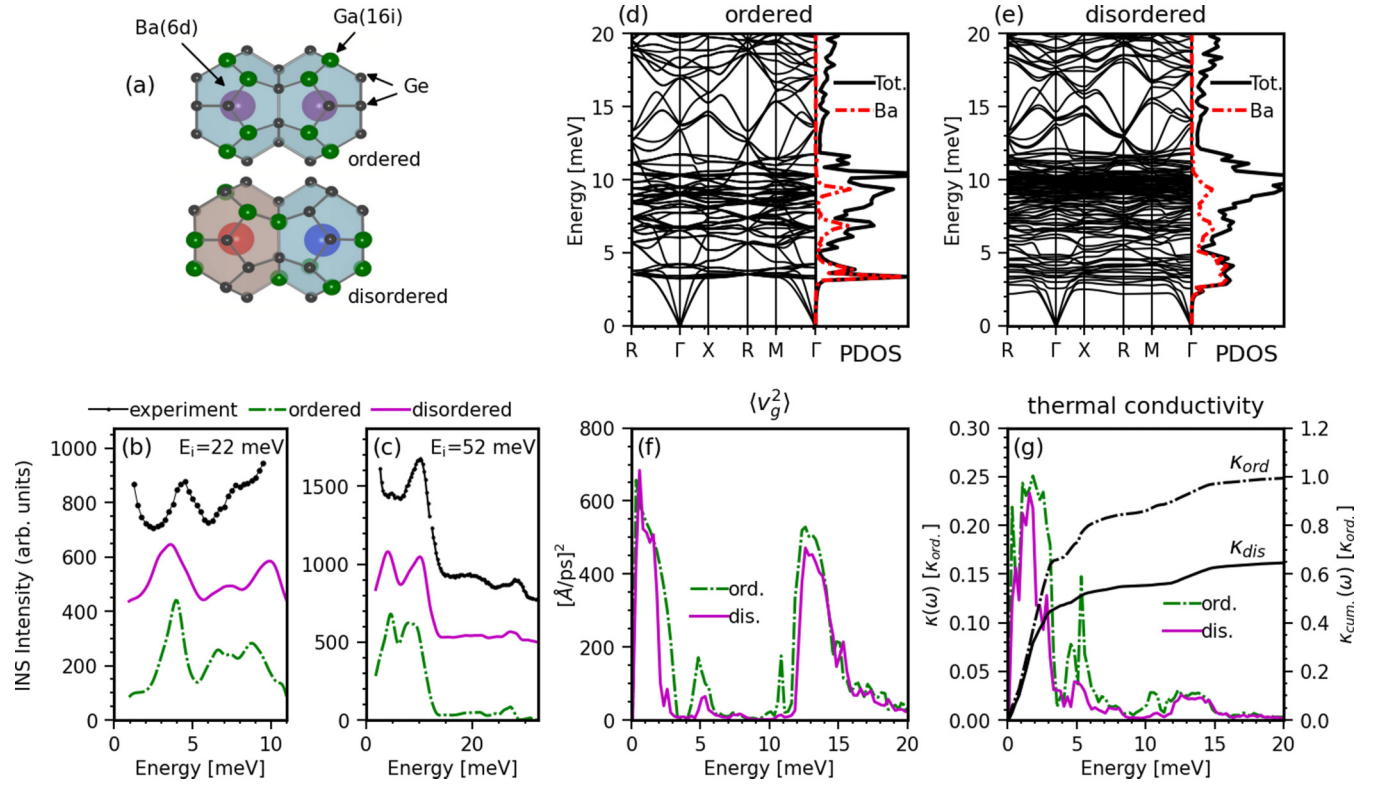
*dmitry.reznik@colorado.edu

FIG. 1. Summary of the lattice dynamical phenomena considered in this Research Letter. (a) Ba-6d containing (Ga, Ge)$_{24}$ cage portion of the three-dimensional unit cells of perfectly ordered Ba$_8$Ga$_{16}$Ge$_{30}$ (top) and disordered Ba$_8$Ga$_{16}$Ge$_{30}$ with scrambled Ge and Ga atom occupations (bottom). (b) and (c) Black curves show neutron-weighted densities of states (DOSs) [inelastic neutron scattering (INS) intensities integrated over the $3 < H < 6$, $3 < K < 7$, $4.5 < L < 6.5$ reciprocal lattice units (r.l.u.) region of reciprocal space] measured with incident energy $E_i = 22$ meV (b) and $E_i = 52$ meV (c). The green (purple) lines are the same quantity calculated from DFT using the ordered (disordered) unit cells and broadened with an approximate resolution function fit to the experimental intensity (see Supplemental Material [19]). The disordered calculation and the experimental curves for $E_i = 22$ meV are offset vertically by 350 and 400 counts, respectively. The experimental curve has an additional large (~250 counts) background that is not present in the calculations. For $E_i = 52$ meV, the disordered and experimental curves are offset by 500 and 700 counts, respectively. Here, the experimental background is ~600 counts. (d) and (e) The ordered (d) and disordered (e) phonon dispersions and phonon densities of states (PDOSs). The dash-dotted red curve is the projection onto the Ba atoms; the black curve is the total DOS (Tot.). (f) The average group velocities squared, $\langle v_g^2 \rangle$, calculated from the dispersions in (d) and (e) by averaging over all modes and $\boldsymbol{q}$ points. (g) Colored curves represent the spectral thermal conductivities $\kappa(\omega)$, and black curves represent the cumulative thermal conductivities $\kappa_{\text{cum}}(\omega)$ at 300 K calculated from the group velocities and densities of states in (f) and in (d) and (e). Only umklapp processes are considered; $\tau(\omega) = \tau_0 \omega^{-2}$, with τ_0 being the same for the ordered (ord.) and disordered (dis.) calculations. The data in (g) are in units of the total thermal conductivity of the ordered crystal.

occupational disorder control represents an alternative direction in the design of thermoelectric materials based on clathrates.

Neutron scattering measurements were performed on the Merlin direct geometry chopper spectrometer at the ISIS Neutron and Muon Source at the Rutherford Appleton Laboratory in Didcot, United Kingdom [20]. The Ba$_8$Ga$_{16}$Ge$_{30}$ crystal used for the inelastic neutron scattering experiment is the same sample that was used in Ref. [21]. Merlin has high flux and a large detector area, collecting the four-dimensional inelastic neutron scattering data set S($\mathbf{Q}, \omega$) across many Brillouin zones (BZs). For data analysis, we used the PHONON EXPLORER software [22,23], which enables an efficient search for wave vectors where a particular effect is observed most clearly and performs multizone fitting to efficiently separate phonon branches that are much more closely spaced than the experimental resolution [24]. We used PHONOPY to solve the lattice dynamical equations based on the force constants from

Ref. [25]. The inelastic neutron scattering structure factors, S($\mathbf{Q}, \omega$), were simulated using the Simulating Neutron and X-ray Scans (SNAXS) [26] and EUPHONIC [27] software. To represent the finite linewidths and experimental resolution broadening, the structure factors in Figs. 2 and 3 were convoluted with a Gaussian function assuming that the full width at half maximum (FWHM) is 0.75 meV. The intensity scales in arbitrary units for all S($\mathbf{Q}, \omega$) calculations are the same.

The ordered phase of Ba$_8$Ga$_{16}$Ge$_{30}$ typically used in DFT calculations [Fig. 1(a), top] has cubic symmetry, and intensities along reciprocal lattice directions with permuted axes are identical. On the other hand, the real structure of Ba$_8$Ga$_{16}$Ge$_{30}$ is disordered with Ga and Ge atoms randomly distributed on the cage vertices [Fig. 1(a), bottom] [14–18,25]. The disorder breaks the cubic symmetry (Pm-$3n \rightarrow P1$), and intensities along directions that are equivalent in the ordered crystal are no longer identical. Still, the experimental S($\mathbf{Q}, \omega$) is averaged over the large number (~10^{23}) of different disordered
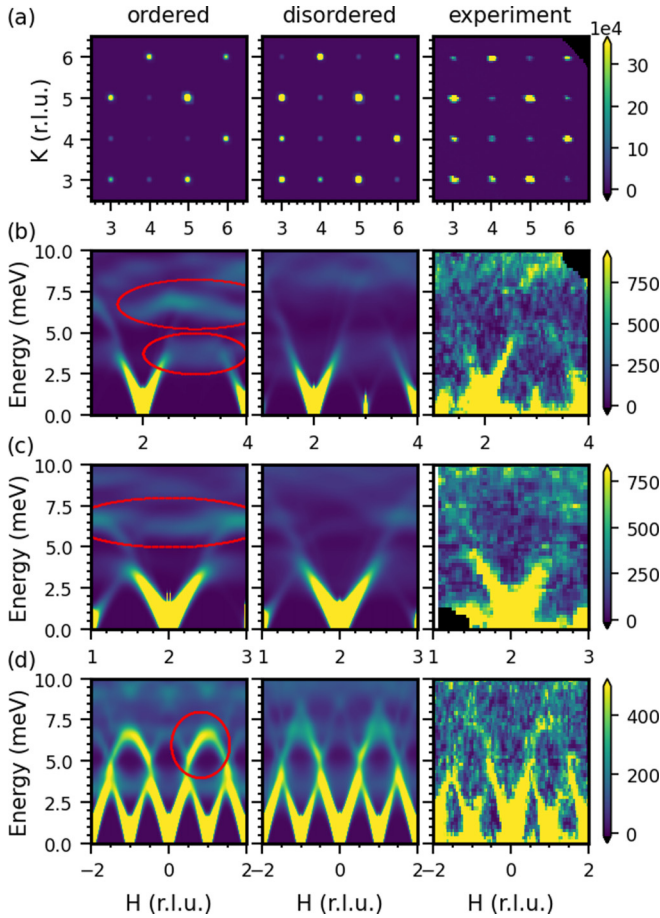
FIG. 2. Ordered (left column) and disordered (middle column) neutron spectra compared with experiment (right column). (a) Bragg peaks $(-1 < E < 1$ meV) in the $(H, K, L = 6)$ plane. In the ordered cell, coherent scattering from the ordered arrangement of atoms results in certain Bragg peaks [e.g., $\mathbf{Q} = (4, 4, 6)$] having no intensity. On the other hand, scattering from the disordered arrangement of atoms results in some remaining intensity at these Bragg peaks, in excellent agreement with the experimental Bragg pattern. (b)–(d) The remaining rows show inelastic scattering spectra $S(\mathbf{Q}, \omega)$ along the $\mathbf{Q} = (H, 6, 6)$ (b), $\mathbf{Q} = (H, 2, 8)$ (c), and $\mathbf{Q} = (H, 5, 3)$ (d) reciprocal lattice directions. The disordered calculation is averaged over all otherwise equivalent directions as explained in the text. Red ovals in the ordered calculation indicate intensity from excitations that is not visible in the disordered calculation and experiment as discussed below.

unit cell configurations of the macroscopic crystal, which results in an apparent cubic symmetry.

In DFT the force constants of $Ba_8Ga_{16}Ge_{30}$ were calculated from a single unit cell in both the ordered and disordered phases [25] because $Ba_8Ga_{16}Ge_{30}$ has a large enough unit cell that force constants fall off sufficiently at the cell boundary. Still, disorder breaks translational symmetry, so the computational unit cell should be sufficiently large that atoms on opposite sides of the cell are uncorrelated. Moreover, one should calculate phonons using an ensemble of disordered configurations and average over all ensembles. However, this is too computationally expensive in our case.
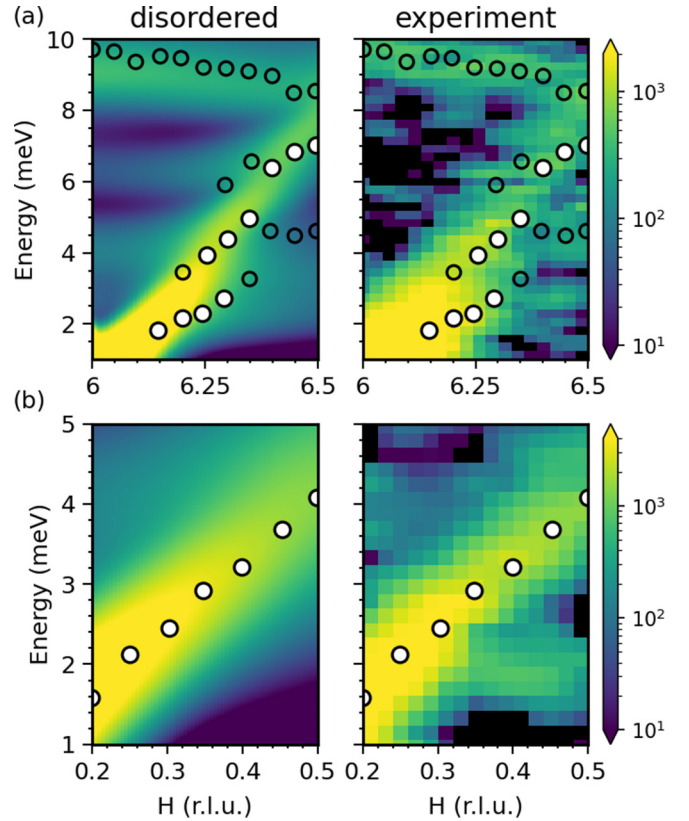

FIG. 3. (a) LA and (b) TA phonon scattering intensities (color maps) at $\mathbf{Q} = (5.5 + h, 0, 0)$ (a) and $\mathbf{Q} = (6, h, 0)$ (b) and experimental phonon energies (circles) obtained from the multizone fit of experimental inelastic neutron scattering intensity $S(\mathbf{Q}, \omega)$ (see Fig. S5 of the Supplemental Material). The white-filled circles indicate acoustic phonons, and the open circles are optic modes. We do not include the small intensity near 2.5 meV in our phonon fits as it does not appear in any other zones and may be an artifact.

We calculated $S(\mathbf{Q}, \omega)$ from a single configuration (from Ref. [25]) chosen using the "special quasirandom structure" (SQS) method [28]. The goal of the SQS method is to pick a small computational supercell that best matches the disorder in a very large (ideally infinite) supercell. This was achieved by fitting correlation functions calculated from a single unit cell with scrambled Ge-Ga occupations to true "random" correlation functions; e.g., from experiment or calculated from a very large supercell. The "disorder" (in the case of $Ba_8Ga_{16}Ge_{30}$, the Ga-Ge site occupancies) is varied to minimize the difference between the correlation function(s) of the computational cell and the true random correlation function(s). The structure with the best match was chosen for the calculations. To approximate the implicit directional averaging, the theoretical $S(\mathbf{Q}, \omega)$ calculated from this disordered cell were averaged over all directions that are equivalent assuming cubic symmetry.

Calculation based on the ordered structure gives the optic flat branches bunched into several narrow energy intervals. Projecting the phonon densities of states onto the individual atoms shows primarily Ba-$6d$ character; thus these are the rattler modes of Ba at the $6d$ site. Disorder spreads these branches out in energy [Figs. 1(d) and 1(e)]. In particular, the

ordered calculation gives avoided crossings between acoustic branches and the nearly flat rattler branches near ~4 meV, which tend to reduce the phonon group velocity and, as a consequence, the thermal conductivity. Due to disorder, these avoided crossings become distributed throughout a broad energy interval between 2 and 5 meV, which further suppresses thermal conductivity by a large amount. The main effect of the splitting of the rattler modes is to create additional avoided crossings with the acoustic phonons (see Supplemental Material for a more detailed discussion [19]).

Figures 1(b) and 1(c) show that the calculated phonon density of states (DOS) corrected for the neutron cross section agrees much better with experiment when the disordered structure is used. In both calculations the energy of the lowest DOS peak is about 3 meV compared with 4.5 meV in experiment, consistent with the known tendency of DFT to underestimate the force constants overall. However, the width of this peak, which comes from the gaps at the avoided crossings of acoustic phonons and rattler modes, is increased in the disordered calculation to closely match experiment. Moreover, the calculated Bragg peak intensities agree much better with experiment if disorder is included in the calculation (Fig. 2). The same applies to select phonon spectra [Figs. 2(b)–2(d)]. Color maps of the simulated and background-subtracted experimental spectra of acoustic phonons shown in Fig. 3 are similar, highlighting the accuracy of the calculation. Peak positions obtained from the multizone fit (see Sec. V of the Supplemental Material for details) agree very well with the color maps of both the simulation and the experiment. In particular, signatures of avoided crossings of the longitudinal acoustic (LA) branch with optic modes are clearly visible in the simulation and the data.

Our calculation of thermal conductivity [Figs. 1(f) and 1(g)] considered umklapp scattering only. A more accurate calculation just for the disordered case is reported in Ref. [25]. Figures 1(f) and 1(g) illustrate a profound effect of the disorder, which suppresses phonon thermal conductivity mostly around 3–5 meV, where the effect of the rattler branches is the strongest.

Comparison of our calculations with the Raman results of Ref. [29] shows that broadening of the Raman phonon peaks far beyond the experimental resolution is a natural consequence of disorder-induced splitting of the modes [19].

In $Ba_8Ga_{16}Ge_{30}$ and similar semiconducting clathrates, most DFT calculations investigating the avoided crossing regions assume that the Ga-Ge site occupancies are fully ordered with Ga only in the 16*i* site and Ge in the remaining cage vertex positions [30–35]. However, there is extremely strong evidence that the Ga-Ge occupancies on the cage vertices are disordered [14–18,25]. Unfortunately, modeling disordered materials from first principles greatly increases the computational workload, which has limited the number of studies of the lattice dynamics in clathrates [36,37].

Ikeda *et al.* [25] investigated the *temperature dependence* of the thermal conductivity and specific heat of $Ba_8Ga_{16}Ge_{30}$ with and without disorder. Only when accounting for correlation in a Kondo-like phonon effect could the experimental temperature dependence be explained [25]. They noted that whereas the temperature dependence is robust against disorder, the absolute value of the thermal conductivity is lowered

in the disordered calculation. The decrease was attributed to shorter lifetimes due to increased anharmonicity [25], similar to $Ba_8Ga_{41}Au_5$, where disorder increases the available phase space for three-phonon scattering [38]. Here we showed that another important effect of disorder is to lower the phonon group velocities.

Disorder-induced dispersion flattening was theoretically predicted in $K_8Al_8Si_{38}$, with Al-Si occupational disorder [36]. Another study found that isotope disorder in the guest atom sites in Si_x and Ba_8Si_x ($x \in \{46, 230, 644\}$) played a major role in reducing thermal conductivity [37] due to both lifetime and group velocity reduction. However, these effects have not been confirmed in experiment, which we did here for $Ba_8Ga_{16}Ge_{30}$.

Our ordered cell calculations show that the flat branches in Figs. 2 and 3 near ~4 and ~6 meV come mainly from pure Ba guest atom modes (see Fig. 1 and the atom-projected INS intensities in the Supplemental Material [19]). These multiply degenerate branches all contribute some intensity to the spectrum. Their intensities appear as a weak but visible flat branch across the BZ (red ovals in Fig. 2). It also shows up as a narrow, pronounced peak in the ordered cell neutron-weighted DOS in Fig. 1. However, the absence of this intensity in the experiment above the background and the significantly improved agreement of the Bragg patterns of the disordered cell over the ordered cell necessitate the disordered calculation.

In the disordered cell calculations, broken symmetry splits the Ba rattler atom branches. Since the wave vectors **Q** with permuted axes are no longer equivalent, $S(\mathbf{Q}, \omega)$ is averaged over all equivalent cubic directions in the simulation suppressing and broadening the simulated intensity of the flat modes. As a result, the only substantial intensity is near the acoustic branches, consistent with experiment. The sharp, pronounced peaks near ~4 and ~6 meV in the neutron-weighted DOS (Fig. 1) become broad and flat when calculated from the disordered cell. Notably, the neutron-weighted DOS curve calculated from the disordered cell agrees with the experimental data much better than the simulation without disorder.

In $Ba_8Ga_{16}Ge_{30}$, an avoided crossing between an acoustic phonon mode and the flat guest modes was theoretically predicted, and it was claimed that the Ba guest atoms behave as local resonating scattering centers for the acoustic phonon modes in the region of the avoided crossing [39]. Subsequent triple-axis neutron scattering measurements along the [*hh*0] direction [21] found that the Ba rattler atoms flatten the phonon dispersions, reducing the group velocity v, rather than acting as a local resonant scattering center and reducing τ. In our data focusing on the [*h*00] direction, large-gap avoided crossings with different well-separated rattler atom branches are apparent in the LA phonon dispersion [Fig. 3(a)]. Meanwhile, the intensity in Fig. 3(b) depicts a transverse acoustic (TA) mode that is linear and continuously dispersing in both the experiment and in the simulation based on the disordered calculation. However, our DFT calculations predict many "small-gap" avoided crossings near ~4 and ~6 meV that are washed out by the instrument resolution both in the experiment and in the simulation for both the TA branch and, away from the large-gap avoided crossings, the LA branch.

Ga and Ge differ in nuclear charge and mass by only ~3.5%, so the perturbation to the force constants induced

by mass or nuclear-charge disorder is insignificant. However, the bonds formed with Ga and Ge have different valence configurations. The electronic structure, which affects the Born-Oppenheimer electronic-energy part of the interatomic force constants, is thus qualitatively different between the ordered and disordered configurations. The impact of disorder can be seen in the substantially lowered average group velocities due to small-gap avoided crossings, between ~ 2 and ~ 4 meV in Fig. 1. (See also the Supplemental Material for a heuristic explanation of this concept [19].) Regardless of any reductions in τ (which are probably also present [25]), the velocity v in the kinetic theory model is substantially reduced, which might explain the anomalously low thermal conductivity in $Ba_8Ga_{16}Ge_{30}$.

To conclude, our calculations using the disordered unit cell validated by experiments show that Ga-Ge occupational disorder has a large effect on phonon dispersions through a strong influence on the electronic structure that underlies interatomic force constants. The disorder introduces many closely spaced optic branches with many more avoided crossings with acoustic modes. These small gaps are essential for understanding the observed low thermal conductivity of $Ba_8Ga_{16}Ge_{30}$ and other similar materials.

[1] G. J. Snyder and E. S. Toberer, Complex thermoelectric materials, Nat. Mater. **7**, 105 (2008).

[2] X. Zhang and L.-D. Zhao, Thermoelectric materials: Energy conversion between heat and electricity, J. Materiomics **1**, 92 (2015).

[3] J. M. Ziman, *Principles of the Theory of Solids* (Cambridge University Press, Cambridge, 1972).

[4] R. Chasmar and R. Stratton, The thermoelectric figure of merit and its relation to thermoelectric generators, J. Electron. Control **7**, 52 (1959).

[5] *CRC Handbook of Thermoelectrics*, edited by D. M. Rowe *et al.*, (CRC Press, Boca Raton, FL, 1995).

[6] G. Nolas, J. Cohn, G. Slack, and S. Schujman, Semiconducting Ge clathrates: Promising candidates for thermoelectric applications, Appl. Phys. Lett. **73**, 178 (1998).

[7] V. Keppens, D. Mandrus, B. C. Sales, B. Chakoumakos, P. Dai, R. Coldea, M. Maple, D. Gajewski, E. Freeman, and S. Bennington, Localized vibrational modes in metallic solids, Nature (London) **395**, 876 (1998).

[8] K. F. Hsu, S. Loo, F. Guo, W. Chen, J. S. Dyck, C. Uher, T. Hogan, E. Polychroniadis, and M. G. Kanatzidis, Cubic AgPb$_m$SbTe$_{2+m}$: Bulk thermoelectric materials with high figure of merit, Science **303**, 818 (2004).

[9] P. F. Poudeu, J. D'Angelo, A. D. Downey, J. L. Short, T. P. Hogan, and M. G. Kanatzidis, High thermoelectric figure of merit and nanostructuring in bulk p-type Na$_{1-x}$Pb$_m$Sb$_y$Te$_{m+2}$, Angew. Chem., Int. Ed. **45**, 3835 (2006).

[10] A. Bentien, M. Christensen, J. D. Bryan, A. Sanchez, S. Paschen, F. Steglich, G. D. Stucky, and B. B. Iversen, Thermal conductivity of thermoelectric clathrates, Phys. Rev. B **69**, 045107 (2004).

[11] J. L. Cohn, G. S. Nolas, V. Fessatidis, T. H. Metcalf, and G. A. Slack, Glasslike Heat Conduction in High-Mobility Crystalline Semiconductors, Phys. Rev. Lett. **82**, 779 (1999).

[12] K. A. Kovnir and A. V. Shevelkov, Semiconducting clathrates: Synthesis, structure and properties, Russ. Chem. Rev. **73**, 923 (2004).

[13] E. S. Toberer, A. F. May, and G. J. Snyder, Zintl chemistry for designing high efficiency thermoelectric materials, Chem. Mater. **22**, 624 (2010).

[14] B. Chakoumakos, B. Sales, and D. Mandrus, Structural disorder and magnetism of the semiconducting clathrate Eu$_8$Ga$_{16}$Ge$_{30}$, J. Alloys Compd. **322**, 127 (2001).

[15] M. Christensen, N. Lock, J. Overgaard, and B. B. Iversen, Crystal structures of thermoelectric n-and p-type Ba$_8$Ga$_{16}$Ge$_{30}$ studied by single crystal, multitemperature, neutron diffraction, conventional X-ray diffraction and resonant synchrotron X-ray diffraction, J. Am. Chem. Soc. **128**, 15657 (2006).

[16] A. Bentien, A. E. Palmqvist, J. D. Bryan, S. Latturner, G. D. Stucky, L. Furenlid, and B. B. Iversen, Experimental charge densities of semiconducting cage structures containing alkaline earth guest atoms, Angew. Chem. **112**, 3759 (2000).

[17] A. Bentien, E. Nishibori, S. Paschen, and B. B. Iversen, Crystal structures, atomic vibration, and disorder of the type-I thermoelectric clathrates Ba$_8$Ga$_{16}$Si$_{30}$, Ba$_8$Ga$_{16}$Ge$_{30}$, Ba$_8$In$_{16}$Ge$_{30}$, and Sr$_8$Ga$_{16}$Ge$_{30}$, Phys. Rev. B **71**, 144107 (2005).

[18] A. Bentien, B. Iversen, J. Bryan, G. Stucky, A. Palmqvist, A. Schultz, and R. Henning, Maximum entropy method analysis of thermal motion and disorder in thermoelectric clathrate Ba$_8$Ga$_{16}$Si$_{30}$, J. Appl. Phys. **91**, 5694 (2002).

[19] See Supplemental Material at http://link.aps.org/supplemental/10.1103/PhysRevB.107.L020301 for a discussion of atom-projected neutron scattering intensities and other supporting information.

[20] R. I. Bewley, R. S. Eccleston, K. A. McEwen, S. M. Hayden, M. T. Dove, S. M. Bennington, J. R. Treadgold, and R. L. S. Coleman, MERLIN, a new high count rate spectrometer at ISIS, Physica B (Amsterdam) **385-386**, 1029 (2006).

[21] M. Christensen, A. B. Abrahamsen, N. B. Christensen, F. Juranyi, N. H. Andersen, K. Lefmann, J. Andreasson, C. R. Bahl, and B. B. Iversen, Avoided crossing of rattler modes in thermoelectric materials, Nat. Mater. **7**, 811 (2008).

[22] D. Reznik, Phonon-explorer, https://github.com/dmitryr1234/Phonon-Explorer.

[23] D. Reznik and I. Ahmadova, Automating analysis of neutron scattering time-of-flight single crystal phonon data, Quantum Beam Sci. **4**, 41 (2020).

[24] D. Parshall, R. Heid, J. L. Niedziela, T. Wolf, M. B. Stone, D. L. Abernathy, and D. Reznik, Phonon spectrum of SrFe$_2$As$_2$

determined using multizone phonon refinement, Phys. Rev. B **89**, 064310 (2014).

[25] M. Ikeda, H. Euchner, X. Yan, P. Tomeš, A. Prokofiev, L. Prochaska, G. Lientschnig, R. Svagera, S. Hartmann, E. Gati, M. Lang, and S. Paschen, Kondo-like phonon scattering in thermoelectric clathrates, Nat. Commun. **10**, 887 (2019).

[26] D. Parshall, Simulating neutron and x-ray scans, https://github.com/danparshall/snaxs.

[27] R. L. Fair, A. J. Jackson, D. J. Voneshen, D. B. Jochym, M. D. Le, K. Refson, and T. G. Perring, Euphonic inelastic neutron scattering simulations from force constants and visualization tools for phonon properties, J. Appl. Cryst. **55**, 1689 (2022).

[28] A. Zunger, S.-H. Wei, L. G. Ferreira, and J. E. Bernard, Special Quasirandom Structures, Phys. Rev. Lett. **65**, 353 (1990).

[29] Y. Takasu, T. Hasegawa, N. Ogita, M. Udagawa, M. A. Avila, K. Suekuni, I. Ishii, T. Suzuki, and T. Takabatake, Dynamical properties of guest ions in the type-I clathrate compounds $X_8Ga_{16}Ge_{30}(X = Eu, Sr, Ba)$ investigated by Raman scattering, Phys. Rev. B **74**, 174303 (2006).

[30] T. Tadano, Y. Gohda, and S. Tsuneyuki, Impact of Rattlers on Thermal Conductivity of a Thermoelectric Clathrate: A First-Principles Study, Phys. Rev. Lett. **114**, 095501 (2015).

[31] H. Euchner and A. Groß, Predicting accurate phonon spectra: An improved description of lattice dynamics in thermoelectric clathrates based on the SCAN meta-GGA functional, Chem. Mater. **31**, 2571 (2019).

[32] R. L. González-Romero and A. Antonelli, Estimating carrier relaxation times in the $Ba_8Ga_{16}Ge_{30}$ clathrate in the extrinsic regime, Phys. Chem. Chem. Phys. **19**, 3010 (2017).

[33] T. Tadano and S. Tsuneyuki, Quartic Anharmonicity of Rattlers and Its Effect on Lattice Thermal Conductivity of Clathrates from First Principles, Phys. Rev. Lett. **120**, 105901 (2018).

[34] N. P. Blake, L. Møllnitz, G. Kresse, and H. Metiu, Why clathrates are good thermoelectrics: A theoretical study of $Sr_8Ga_{16}Ge_{30}$, J. Chem. Phys. **111**, 3133 (1999).

[35] J. Dong, O. F. Sankey, G. K. Ramachandran, and P. F. McMillan, Chemical trends of the rattling phonon modes in alloyed germanium clathrates, J. Appl. Phys. **87**, 7726 (2000).

[36] Y. He and G. Galli, Nanostructured clathrate phonon glasses: Beyond the rattling concept, Nano Lett. **14**, 2920 (2014).

[37] Y. Gao, X. Zhang, Y. Zhou, and M. Hu, Giant reduction in thermal conductivity of extended type-I silicon clathrates and prominent thermal effect of 6d guest Wyckoff positions, J. Mater. Chem. C **5**, 10578 (2017).

[38] P.-F. Lory, S. Pailhes, V. M. Giordano, H. Euchner, H. D. Nguyen, R. Ramlau, H. Borrmann, M. Schmidt, M. Baitinger, M. Ikeda, P. Tomeš, M. Mihalkovič, C. Allio, M. R. Johnson, H. Schober, Y. Sidis, F. Bourdarot, L. P. Regnault, J. Ollivier, S. Paschen *et al.*, Direct measurement of individual phonon lifetimes in the clathrate compound $Ba_{7.81}Ge_{40.67}Au_{5.33}$, Nat. Commun. **8**, 491 (2017).

[39] J. Dong, O. F. Sankey, and C. W. Myles, Theoretical Study of the Lattice Thermal Conductivity in Ge Framework Semiconductors, Phys. Rev. Lett. **86**, 2361 (2001).